

# Influence of directional solidification variables on the microstructure and crystal orientation of AM3 under high thermal gradient

Xinbao Zhao · Lin Liu · Zhuhuan Yu · Weiguo Zhang · Jun Zhang · Hengzhi Fu

Received: 24 March 2010 / Accepted: 4 June 2010 / Published online: 15 June 2010  
© Springer Science+Business Media, LLC 2010

**Abstract** Solid–liquid interface morphologies of a nickel-base single crystal superalloy AM3 were investigated under high thermal gradient. The critical velocities of planar–cellular and cellular–dendritic transition were greatly increased by high thermal gradients. A high thermal gradient was of great benefit to dendrite refinement. Experimental results showed that the primary and secondary dendrite arm spacings decreased with increasing cooling rate. As expected, the segregation of elements was suppressed and the size of the gamma prime ( $\gamma'$ ) phase decreased significantly with increasing withdrawal rates. The shape of  $\gamma'$  in interdendritic region kept cuboidal at higher withdrawal rate. It was found that the withdrawal rates had little influence on the crystallographic orientation in high thermal gradient directional solidification.

## Introduction

In the past years, directional solidification (DS) techniques were successfully applied to the production of single crystal blades, which has been extensively used in aero-engines [1, 2]. The aims of producing single crystal blades are to eliminate grain boundaries that limit creep rupture properties and to ensure [001] orientation growth with minimum of Young's modulus. However, the DS process is so complex that the formation of cellular and dendritic structures with concomitant microsegregation and misorientation is deleterious since these solidification features

influence mechanical properties obviously. Complicated morphologies of directional solidification structures attract a lot of theoretical studies. Numerical simulations have been used to evaluate the directional solidification for columnar-to-equiaxed transition [3], dendrite growth [4], Tang and Xue [5] introduced the interface evolution of directional solidification of a binary alloy with different boundary heat fluxes by phase-field method. Also, numerous studies [6–8] have reported the dendrite arm spacing as a function of the processing parameters. In DS, the thermal gradient ( $G$ ) and cooling rate ( $GV$ ) are two of the most important factors, which affect the interface morphology and dendrite growth characteristics [9]. However, for industrial as-castings, large single crystal components for industrial gas turbines (IGT) and conventional cooling method (for instance, high rate solidification technique (HRS)) lead to a limited thermal gradient less than 100 K/cm [10, 11]. Low thermal gradient results in coarse-dendrite and severe segregation, which greatly influence the performance of the castings. In recent years, the development of liquid metal cooling (LMC) has significantly improved the thermal gradient. Researches [12, 13] show that fine dendrites could be obtained under a high cooling rate with high thermal gradient.

With increasing cooling rate, the solid–liquid interface changes from planar to cellular, and then to dendritic morphology. The transition velocities are greatly dependent on  $G$  and  $GV$  in directional solidification, so that the investigation of the morphology evolution under high thermal gradient is important. It is known that the preferred orientation of nickel-base superalloys is  $\langle 001 \rangle$ , which has the smallest Young's modulus [14, 15]. During the growth of turbine blades, off-axial orientations may occur and usually deviate from  $\langle 001 \rangle$  by up 12°–15°, even in the case of planar growth. The deviation of crystallographic

X. Zhao (✉) · L. Liu · Z. Yu · W. Zhang · J. Zhang · H. Fu  
State Key Laboratory of Solidification Processing,  
Northwestern Polytechnical University, Xi'an 710072,  
People's Republic of China  
e-mail: zhxb001@163.com

orientation greatly influences the mechanical properties. Most of the engineers recognize that the crystals with misorientation less than  $5^\circ$  or  $10^\circ$  can be acceptable [16]. Therefore, the effect of withdrawal rate on crystal orientation under high thermal gradient should be clarified.

The aim of this work is to study the influence of the withdrawal rate on the interface morphologies and microstructures in a directionally solidified superalloy under high thermal gradient. The changes of the crystal orientation during the directional solidification are also discussed.

## Experimental

DS experiments were performed on a nickel-based superalloy AM3. The chemical compositions in weight percents were: Cr 7.82, Co 5.34, Mo 2.25, W 4.88, Al 6.02, Ti 1.94, Ta 3.49, C 0.006, and Ni balanced. Cylindrical samples were cut with 4 mm in diameter. In the directional solidification process, samples were heated by a dual resistant heating technique and cooled by melting liquid metals to obtain higher thermal gradient. Single crystals were obtained by remelting the alloy followed by growth with the bottom seeding technique. The thermal gradient at the solid–liquid interface was measured to be 360 K/cm. The withdrawal rates were selected to be eight different values: 3.5, 6, 10, 50, 100, 200, 400, and 600  $\mu\text{m/s}$ . The  $\langle 001 \rangle$  orientation of the seed was prearranged to keep a constant misorientation of  $8^\circ$  distant from the cylindrical axis.

The samples were etched in a solution composed of 14 mL HCl, 21 mL  $\text{H}_2\text{O}$ , and 8 g  $\text{FeCl}_3$  for optical observation. The observation was carried out using a LEICA DM4000M microscope. The primary and secondary dendrite arm spacings ( $\lambda_1$  and  $\lambda_2$ ) were measured in transverse planes and longitudinal planes, respectively. Quantitative analyzing of the microstructures was performed by Sisc IAS V8.0 image analysis system. The triangle method was used by joining the three neighbor dendrite centers and sides of the triangle [17,18]. In this way, at least 200  $\lambda_1$  values and more than 50  $\lambda_2$  were measured for each specimen. Each of the value reported here was the calculated average value. At the same time, the errors of the values were calculated. The microstructure was examined after etching by another corrosive (nitric acid: hydrofluoric acid: glycerin = 1:2:3) using scanning electron microscope (SEM, ZEISS SUPRA 55). The size of  $\gamma'$  phase was determined by  $A = \sqrt{S_T/n}$ , where  $S_T$  is accumulative total  $\gamma'$  area of whole viewing field of micrograph (in dendrite core or interdendrite) and  $n$  is the number of  $\gamma'$  variation. X-ray diffraction (XRD) analysis was employed for the identification of the crystal orientation which was described elsewhere [19]. The concentrations of the elements in the dendrite core and interdendritic

regions were determined on a JAX-8100 electron probe microanalysis (EPMA). Line scans were performed to measure the compositions [20], and the intervals points of measured points were chosen as 10  $\mu\text{m}$  along the lines.

## Results and discussion

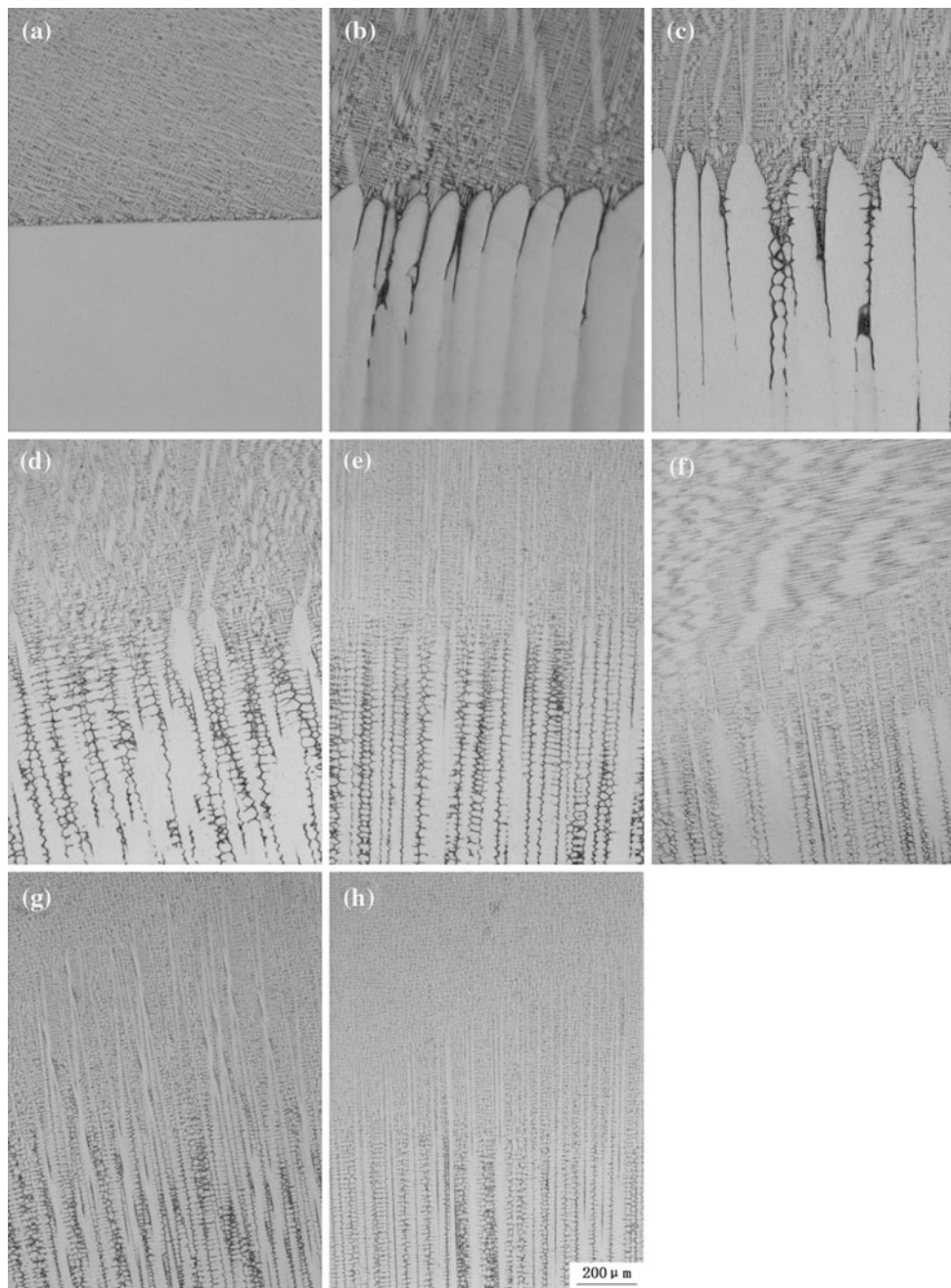
### The evolution of interface morphologies

Figure 1 shows typical interface morphologies in longitudinal sections of samples under high thermal gradient. Planar and cellular interface are observed at withdrawal rates of 3.5 and 6  $\mu\text{m/s}$ , respectively. The interface morphologies change in the sequence of cellular–dendrite, coarse-dendrite, and fine-dendrite with increasing withdrawal rates, as shown in Fig. 1a–h. At withdrawal rates lower than 4  $\mu\text{m/s}$ , the crystal solidified with planar interface. It is noteworthy that most of previous works [21, 22] found that the critical velocity for planar–cellular transition was less than 2  $\mu\text{m/s}$  for the first generation single crystal superalloys in conventional thermal gradient system, indicating that high thermal gradient can stabilize the solidification interface. At a solidification rate of 10  $\mu\text{m/s}$ , the cellular crystal became unstable, then cellular–dendritic transition occurred, meanwhile some side arms appeared at the edge of the cellular trucks. At rates of 4–10  $\mu\text{m/s}$ , solid–liquid interface showed cellular morphology. As expected, the dendrites became smaller as the withdrawal rate increased. It must be pointed out that superfine dendrites can only form under high thermal gradient and large withdrawal rate.

### The dendrite arm spacings

Table 1 shows the values of  $\lambda_1$  and  $\lambda_2$  with increasing withdrawal rate. As expected, the minimum spacing for both primary and secondary dendrite arms was observed in samples with the most rapid withdrawal rate. It showed that  $\lambda_1$  firstly increased, then decreased, and its maximum value occurred at cellular–dendritic interface. The value of  $\lambda_2$  decreased with increasing cooling rate. The superfine structure can be found when the withdrawal rate reached 600  $\mu\text{m/s}$ . The values of  $\lambda_1$  and  $\lambda_2$  were 51 and 12  $\mu\text{m}$ , respectively, which were much smaller than that of the dendrite produced by conventional HRS process.

Dendrite arm spacing is an indication of casting quality in directionally solidified structures. In the past, the average spacings of dendrites or cells for lots of alloys have been measured. Many analytical models have been established [6, 7, 23]. The widely accepted relationship for  $\lambda_1$  as a function of  $G$  and  $V$  is concluded that



**Fig. 1** Solid–liquid interfacial morphologies under various withdrawal rates **a**  $V = 3.5 \mu\text{m/s}$ , **b**  $V = 6 \mu\text{m/s}$ , **c**  $V = 10 \mu\text{m/s}$ , **d**  $V = 50 \mu\text{m/s}$ , **e**  $V = 100 \mu\text{m/s}$ , **f**  $V = 200 \mu\text{m/s}$ , **g**  $V = 400 \mu\text{m/s}$ , **h**  $V = 600 \mu\text{m/s}$

**Table 1** Values of  $\lambda_1$  and  $\lambda_2$  at different withdrawal rate

$V, \mu\text{m/s}$	6	10	50	100	200	400	600
$\lambda_1, \mu\text{m}$	122	138	116	102	78	59	51
$\lambda_2, \mu\text{m}$	–	46	23	21	16	13	12

$$\lambda_1 \propto G^{1/2} \times V^{1/4} \tag{1}$$

For the present experiment, Fig. 2 shows the dependence of  $\lambda_1$  as a function of  $G$  and  $V$ .

Guo et al. [22] and Du [24] had investigated the effect of solidification cooling rate on  $\lambda_1$  on NASAIR 100 and CMSX-2, respectively. Similar results showed that the primary dendrite arm spacing decreased with increased cooling rate. In the cellular growth process,  $\lambda_1$  increased with the cooling rate. However,  $\lambda_1$  decreased with increased cooling rate. There existed a maximum value at the cellular to dendritic transition range.

Compared with the conventional directional solidification systems, the LMC technique greatly increased the

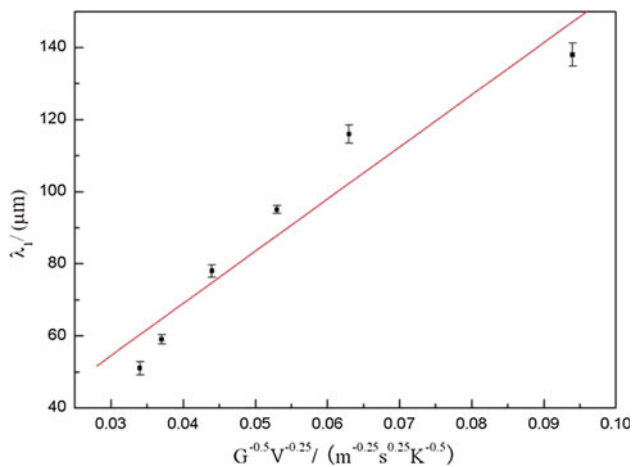


**Fig. 2** Measured primary dendrite arm spacing  $\lambda_1$  plotted as a function of the product of  $G^{-0.5}V^{-0.25}$

**Table 2** Influence of increasing thermal gradient  $G$  on the primary dendrite arm spacing  $\lambda_1$

Alloy	$G$ (K/cm)	$V$ ( $\mu\text{m/s}$ )	$\lambda_1$ ( $\mu\text{m}$ )	Reference
PWA-1484	30	100	440	[25]
PWA-1480	90	100	215	[26]
AM3	360	100	102	This work
CMSX-2	1000	100	38	[13]

thermal gradient of the solid–liquid interface. At a constant withdrawal rate, the primary dendrite arm spacing decreased significantly with the increased  $G$ , as shown in Table 2. Quedsted et al. [27] have found that with increasing  $G$  and  $GV$ , it would be possible to obtain better performance for high Cr superalloy.

#### Microsegregation of the dendrite structure

Figure 3 shows the segregation behavior of alloying elements in the crystals with increasing withdrawal rate. A segregation coefficient  $k'$  is usually defined as the ratio of the concentration of the element in the dendrite core to that

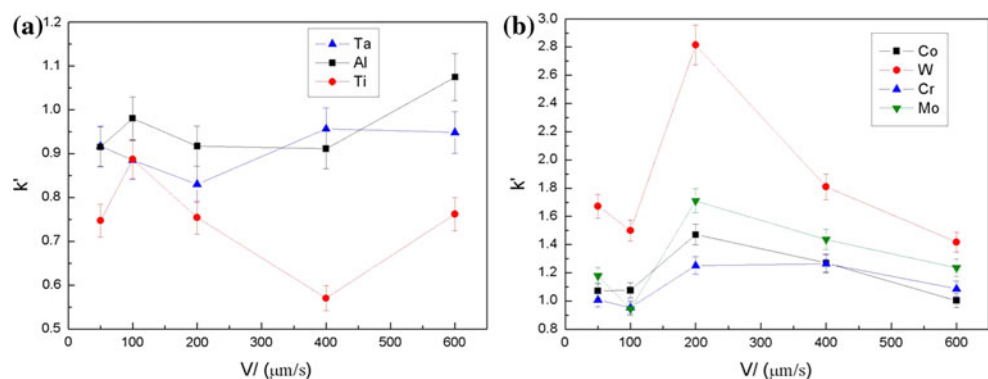
in the interdendritic region. The value of  $k'$  less than 1 indicates that the elements segregated to the interdendritic regions and these elements are positive segregation elements. While  $k'$  values greater than 1 indicate that the elements segregated to the dendrite cores and these elements are negative segregation elements. With smaller segregation coefficient, the degree of segregation to the interdendritic region would be greater. From Fig. 3, it can be seen that Al, Ti, and Ta segregate to interdendritic regions, Co and W segregate to dendrite cores. W has the biggest tendency to partition to dendrite cores.

The inherent characteristics of dendritic solidification are the difference in composition. However, high thermal gradient directional solidification can reduce this difference. All the elements exhibited greater degree of segregation at 200  $\mu\text{m/s}$ . At a withdrawal rate of 600  $\mu\text{m/s}$ , the segregation coefficient of most elements approached to 1, except for W and Ti. Dendritic segregation behavior for W and Ti was less affected by the withdrawal rate, which was similar to the DS IN738LC [28]. The results revealed that the degree of the segregation decreased with the increase of withdrawal rate, which were similar to the research of Liu on the CMSX-2 [13]. However, these results are different from the segregation tendency reported for a third generation single crystal alloy, CMSX-10, were a greater degree of segregation with increasing withdrawal rate [29].

#### The morphologies of $\gamma'$ phase in the dendrite structure

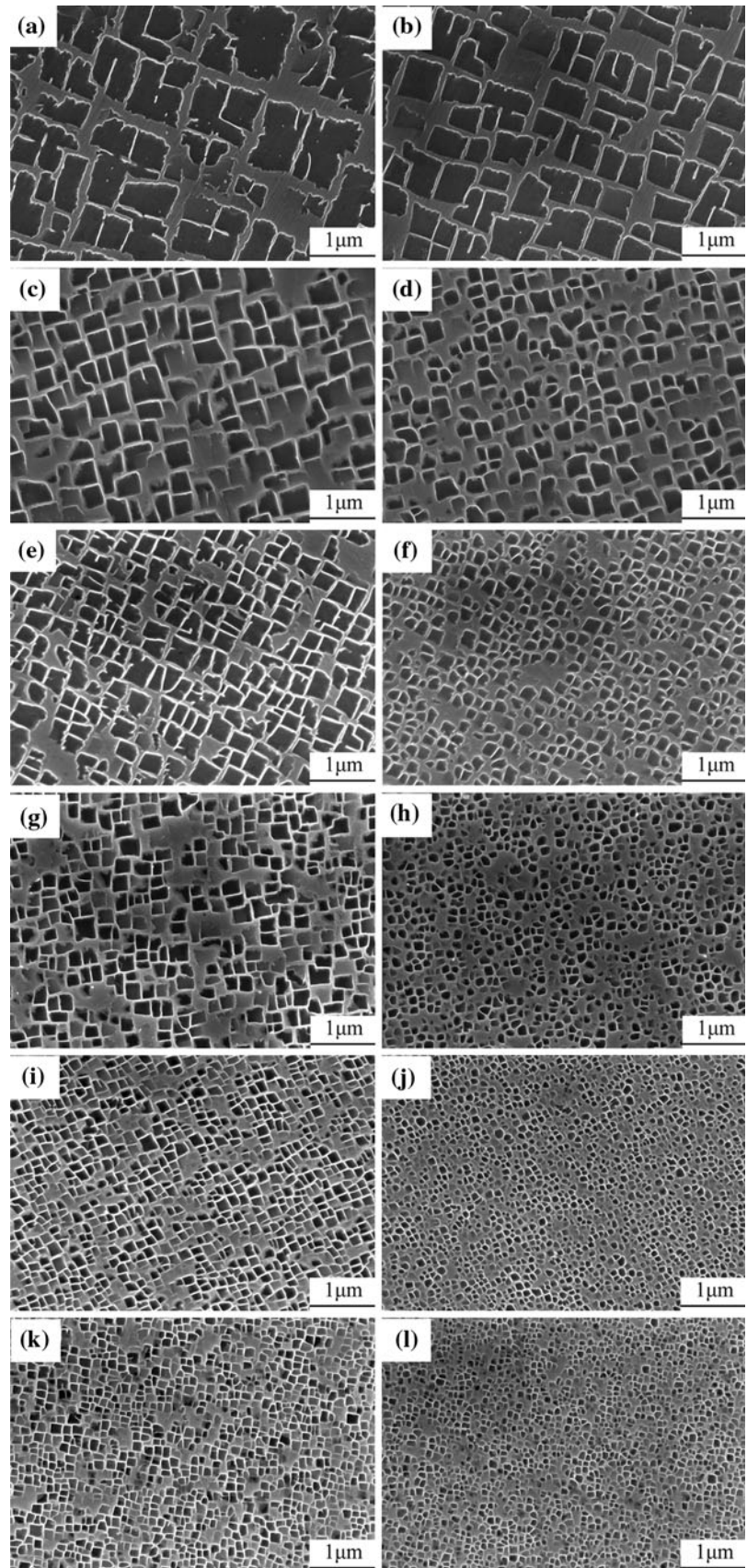
The solidified crystals have a matrix,  $\gamma$  phase, with a disordered face-centered cubic (fcc) structure, containing a dispersion of ordered intermetallic precipitate particles of the type  $\text{Ni}_3(\text{Al}, \text{Ti})$  ( $\gamma'$ ). Figure 4 shows the  $\gamma'$  phase morphologies at different withdrawal rates. Large and cuboidal  $\gamma'$  phase was found in dendrite cores and interdendritic regions at low withdrawal rate. With the increase of withdrawal rate, the  $\gamma'$  phase in the dendrite cores tended to be sphere at the highest withdrawal rate (Fig. 4l), while the  $\gamma'$  phase in the interdendritic regions was still cuboidal (Fig. 4k). This is different from the study of Guo et al. [22],

**Fig. 3** Relationship between segregation coefficient of the elements  $k'$  and withdrawal rate: **a**  $k'$  of positive elements, **b**  $k'$  of negative elements





**Fig. 4** Morphologies of  $\gamma'$  in interdendritic region and dendritic region at different withdrawal rates:  
**a, b**  $V = 10 \mu\text{m/s}$ ,  
**c, d**  $V = 50 \mu\text{m/s}$ ,  
**e, f**  $V = 100 \mu\text{m/s}$ ,  
**g, h**  $V = 200 \mu\text{m/s}$ ,  
**i, j**  $V = 400 \mu\text{m/s}$ ,  
**k, l**  $V = 600 \mu\text{m/s}$ ;  
**a, c, e, g, i, and k** interdendrite,  
**b, d, f, h, j, and l** dendrite core



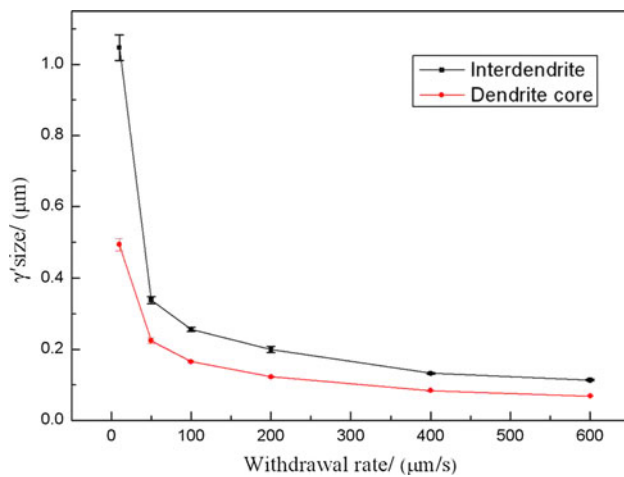


**Fig. 5** Influence of withdrawal rate on the size of  $\gamma'$

which found that the shape of  $\gamma'$  phase tended to be sphere at higher cooling rate. The size of  $\gamma'$  particles decreased with the increasing withdrawal rate, as shown in Fig. 5. Moreover, the size of  $\gamma'$  in the dendrite cores was smaller than that in the interdendritic regions.

The nucleation undercooling of  $\gamma'$  is low at low withdrawal rate, so there are less nuclei and long time for these nuclei to grow. However, with the increasing withdrawal rate, the nucleation undercooling of  $\gamma'$  was increased, which caused a larger number of nuclei and less time to grow. So the size of  $\gamma'$  was decreased at high withdrawal rate. Al, Ti, and Ta are forming elements of  $\gamma'$  phase, which were enriched in interdendritic regions and led to a lower degree of coherency. It is supposed that there is a larger supersaturation, and thus enhanced growth kinetics for  $\gamma'$  in interdendritic regions [30]. Therefore, the size of  $\gamma'$  in interdendritic regions is larger than that in dendritic cores. The initial morphology of  $\gamma'$  is spherical nuclei [22], the  $\gamma'$  in the dendritic cores do not have enough time to ripen and kept spherical at high cooling rate.

#### The variation of crystal orientation

Recent researches on some model alloys have shown that the dendrite growth direction is between heat flow direction of solidification and the preferred orientation of the crystal [31]. In order to investigate the effect of withdrawal rate on the crystal orientation, the preferred orientation of the seed used in the experiments tilted from DS direction about  $8^\circ$ . Figure 6 shows the relationship between withdrawal rate and the crystallographic orientation for single crystal superalloy AM3. It can be seen that the crystallographic orientation had no obvious change with the increasing withdrawal rate. The deviation angle between the preferred orientation and the DS direction had the maximum value at  $400 \mu\text{m/s}$ . It means that higher cooling rate did not result in

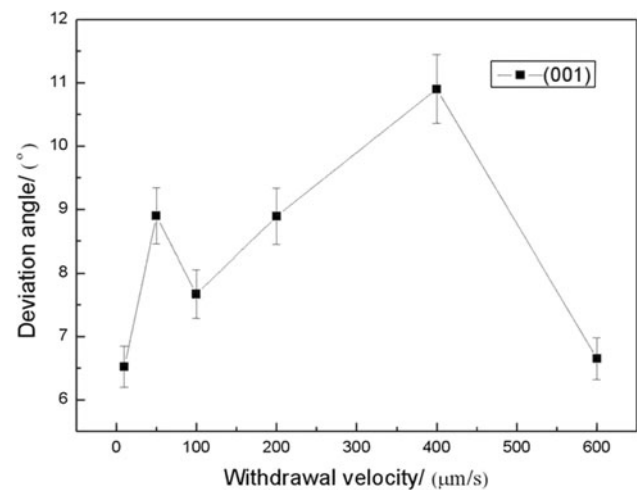


**Fig. 6** Influence of withdrawal rate on crystallographic orientation

larger orientational deviation angle under high thermal gradient. In general, during the process of DS with bottom seeding technique, the orientation of the seed is the one of most important factors to determine the orientation of the single crystal.

#### Conclusions

A series of DS experiments were performed on a multi-component nickel-base superalloy AM3 under high thermal gradient. The microstructure and crystallographic orientation evolution of single crystals were investigated. The following conclusions can be drawn:

- (1) A DS system with high thermal gradient was sufficient to increase the critical interface velocity. The solidification interfaces of AM3 changed in the sequence of planar, cellular, coarse-dendritic and fine-dendritic with increasing withdrawal rate.
- (2) A higher thermal gradient led to smaller dendrite arm spacings. Also, the primary and secondary dendrite arm spacings decreased with increasing withdrawal rate. The microsegregation of the elements was suppressed and the size of  $\gamma'$  decreased at higher cooling rates. The shape of  $\gamma'$  was cuboidal in the interdendritic region while the  $\gamma'$  in the dendrite cores became irregular with the increasing withdrawal rate.
- (3) As the preferred orientation of the seed deviated from the DS direction within  $8^\circ$ , the increased withdrawal rates had little effect on the crystal orientation under high temperature gradient.

**Acknowledgements** The authors would like to thank the National Natural Science Foundation of China (Grant No. 50771081) and the National Basic Research Program of China (2006CB605202) for financial support.

## References

1. Durand-Charre M (1998) The microstructure of superalloys. CRC Press, Boca Raton
2. D'Souza N, Ardakani MG, Mclean M, Shollock BA (2000) Metall Mater Trans A 31:2877
3. Kumar A, Dutta P (2009) J Mater Sci 44:3952. doi:[10.1007/s10853-009-3539-z](https://doi.org/10.1007/s10853-009-3539-z)
4. Madison J, Spowart JE, Rowenhorst DJ, Pollock TM (2008) JOM 60:26
5. Tang JJ, Xue X (2009) J Mater Sci 44:745. doi:[10.1007/s10853-008-3157-1](https://doi.org/10.1007/s10853-008-3157-1)
6. Kurz W, Fisher DJ (1981) Acta Metall 29:11
7. Trivedi R (1984) Metall Trans A 15:977
8. Hunt JD, Lu S-Z (1996) Metall Mater Trans A 27:611
9. Hosch T, England LG, Napolitano RE (2009) J Mater Sci 44:4892. doi:[10.1007/s10853-009-3747-6](https://doi.org/10.1007/s10853-009-3747-6)
10. Clemens ML, Price A, Bellows RS (2003) JOM 55:27
11. Elliott AJ, Tin S, King WT, Huang S-C, Gigliotti MFX, Pollock TM (2004) Metall Mater Trans A 35:3221
12. Fu HZ, Geng XG (2001) Sci Technol Adv Mater 2:197
13. Liu L, Huang TW, Zhang J, Fu HZ (2007) Mater Lett 61:227
14. Caron P, Ohta Y, Nakagawa YG, Khan T (1988) In: Duhl DN et al (eds) Superalloys 1988. The Metallurgical Society, Warrendale, PA, p 215
15. Gunturi SSK, MacLachlan DW, Knowles DW (2000) Mater Sci Eng A 289:289
16. Carter P, Cox DC, Gandin CA, Reed RC (2000) Mater Sci Eng A 280:233
17. Ganesan S, Chan CL, Poirier DR (1992) Mater Sci Eng A 151:97
18. Gündüz M, Çadırlı E (2002) Mater Sci Eng A 327:167
19. Guo ZQ, Fu T, Fu HZ (2000) Mater Charact 44:431
20. Caldwell EC, Fela FJ, Fuchs GE (2004) JOM 56:44
21. Liu L, Zhang J, Huang TW, Fu HZ (2005) Mater Sci Forum 475–479:665
22. Guo XP, Fu HZ, Sun JH (1997) Metall Mater Trans A 28:997
23. Ma D, Sahm P (1998) Metall Mater Trans A 29:1113
24. Du W (1998) Ph.D. Thesis, Northwestern Polytechnical University (in Chinese)
25. Li L, Overfelt RA (2002) J Mater Sci 37:3521. doi:[10.1023/A:1016527509815](https://doi.org/10.1023/A:1016527509815)
26. Vijayakumar M, Tewari SN, Lee JE, Curreri PA (1991) Mater Sci Eng A 132:195
27. Quested PN, McLean M (1980) In: Kirman I et al (eds) Conference on solidification technology in the foundry and cast house. The Metals Society, London, p 586
28. Kermanpur A, Varahraam N, Engilehei E, Mohammadzadeh M, Davami P (2000) Mater Sci Technol 16:579
29. Wilson BC, Cutler ER, Fuchs GE (2008) Mater Sci Eng A 479:256
30. Xiao JM (1987) Alloy phase and phase transformation. Metallurgical Industry Press, Beijing (in Chinese)
31. Esaka H, Daimon H, Natsume Y, Ohsasa K, Tamura M (2002) Mater Trans 43:1312